

Supporting information

A study of recycling reaction system for catalytic transformation of biomass-based carbohydrates via acidic-polar biphasic conditions

Surachai Karnjanakom ^{a*}, Asep Bayu ^d, Panya Maneechakr ^a, Chanatip Samart ^b, Suwadee Kongparakul ^b and Guoqing Guan ^c

^a Department of Chemistry, Faculty of Science, Rangsit University, Pathumthani 12000, Thailand

^b Department of Chemistry, Faculty of Science and Technology, Thammasat University, Pathumthani 12120, Thailand

^c Energy Conversion Engineering Group, Institute of Regional Innovation (IRI), Hirosaki University, 2-1-3, Matsubara, Aomori 030-0813, Japan

^d Research Center for Biotechnology, Indonesian Institute of Sciences (LIPI), Jalan Raya Jakarta-Bogor KM. 46, Cibinong, Bogor, West Java, Indonesia

*Corresponding author.

E-mail addresses: surachai.ka@rsu.ac.th and surachaikarn@gmail.com (S. Karnjanako)

1. Experimental

1.1. Catalyst Characterization

The textural properties such as specific surface area and pore size of catalyst were investigated by N₂ adsorption-desorption isotherms using a Quantachrome Autosorb 1 gas analyzer. Before measurement, the catalyst powder was pretreated at 150 °C for 6 h to remove out moisture and some impurities within the catalyst structure. The surface area and pore size of catalyst were determined by equations of Brunauer–Emmett–Teller (BET) and Barrett–Joyner–Hallenda (BJH), respectively.

The XRD patterns of catalyst structure and crystallinity were recorded using an X-ray diffractometer (Rigaku TTRAX III) in 2 theta range of 10-70° with a scanning step of 0.02° at each point using Cu K α ($\lambda=0.15418$ nm) radiation at 40 kV and 20 mA. The surface morphology of catalyst and the presence of S and Zn elements on catalyst were observed by a scanning electron microscope (SEM S-4800; Hitachi) equipped with energy dispersive spectroscopy (EDS).

The exact amount of Zn on catalyst structure was quantified by inductively coupled plasma atomic emission spectroscopy (ICP-AES). The catalyst acidity was determined by NH₃-Temperature-programmed desorption (NH₃-TPD) using a BEL-CAT analyzer (BEL, Japan). Before measurement, the catalyst powder was preheated at 150 °C for 6 h under He flow (50 ml/min). For NH₃ adsorption procedure, the NH₃ gas (5% of NH₃/He) was adsorbed on catalyst at 40 °C for 1 h with a flow rate of 50 ml/min until it was saturated. Thereafter, NH₃ desorption process was carried out by increasing of temperature from 50 to 500 °C with a heating rate of 3 °C/min. Here, the adsorbed NH₃ concentration was quantified from the peak area by calibration using the standard gas.

Thermal stability of sulfonic group attached on catalyst surface was analyzed using a Thermogravimetric analyzer (Mettler Toledo TGA/SDTA 851). Here, the catalyst powder was heated from 100 to 800 °C at heating rate of 5 °C/min under N₂ flow.

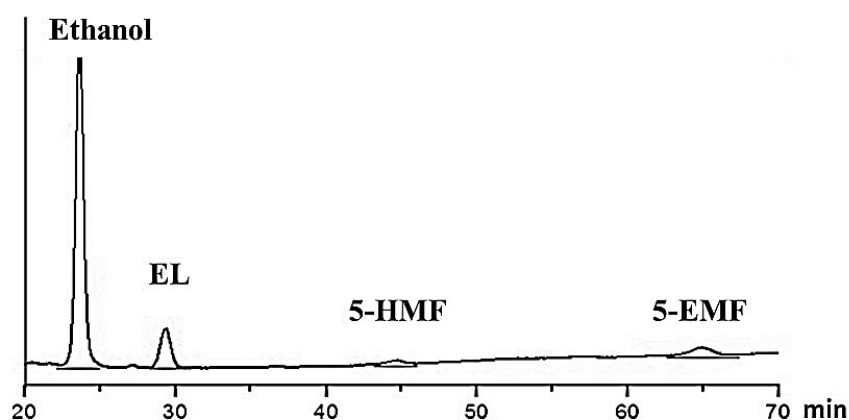
1.2. Analysis of chemical products

The quantitative analyses of 5-HMF, 5-EMF and EL were determined by an Agilent 1200 HPLC chromatograph equipped with and the ultraviolet (UV) detector at 284 nm. The column temperature was maintained at 30 °C, and the mobile phase was water : methanol = 0.8 : 0.2 (v/v). The contents of sucrose, glucose and fructose were analyzed by an Aminex HPX-87H column and Refractive Index (RI) detector. Here, the column temperature was set at 65 °C using 0.05 M sulfuric acid as a mobile phase at a flow rate of 0.55 ml/min. The concentrations of each product were determined based on the external standard method. The amount of zinc ion in liquid sample which leached from Zn-S-C catalyst during reaction was also detected by ICP-AES. To reduce error and ensure its repeatability, each experiment was repeated at least three times under the same conditions. The sucrose conversion and product yield were calculated according to Eqs. (1) and (2):

$$\text{Sucrose conversion (\%)} = \frac{\text{Mole percentage of sucrose reacted}}{\text{Mole percentage of initial sucrose}} \times 100 \quad (1)$$

$$\text{Product yield (\%)} = \frac{\text{Mole percentage of product produced}}{\text{Mole percentage of initial glucose}} \times 100 \quad (2)$$

The example of HPLP chromatogram for product distribution is shown as below:



1.3. Experimental design for EL production from sucrose

Here, Several advantages for these designs have been identified, for instance, (I) it could reduce the error for defining the influence of each parameter and their interactions, (II) the production cost of EL could be significantly decreased since lower number of experiments were carried out by DOE, and (III) much more optimum conditions and response of yield could be obtained when compared with the conventional experiments. The effects of independent input parameters such as catalyst loading amount (X_1), reaction time (X_2), reaction temperature (X_3) and THF amount (X_4) on response of EL yield were investigated to find the significant levels using 2^k factorial design at 95% confidence level. The ranges of factorial design consisting of sixteen experiments with their low (-1) and high (1) levels are shown in Table S1. The regression model for determining the effect of each parameter was provided as follows in Eq. (1):

$$Y = \beta_0 + \sum_{i=1}^k \beta_i X_i + \sum_{i < j} \sum \beta_{ij} X_i X_j \quad (1)$$

Where Y is the percentage of EL yield, β_0 is the intercept/constant coefficient, β_i is the linear coefficients, β_{ij} is the interaction coefficient of each parameter and X_i and X_j are the codes of independent input parameters.

The optimization for production of EL response in this study was designed by using three levels of Box-Behnken model based on quadratic/response surface methodology. This model was defined from combination of factorial with an incomplete block designs, presenting in the shape of a box. Meanwhile, the internal structure of box was assigned by a wire frame which constituted of the edges of the box [1]. The number of experiment in this design were fixed as $N_{\text{exp}} = 2N_p(N_p-1)+N_{\text{cp}}$ where N_{exp} is the number of experiment, N_p is the number of input parameter and N_{cp} is the number of central point. The ranges of this design consisting of

fifteen experiments with their low (-1), medium (0) and high (1) levels are shown in Table S2.

The quadratic model for maximizing the EL yield was provided as follows in Eq. (2):

$$Y = \beta_0 + \beta_1 X_1 + \beta_2 X_2 + \beta_3 X_3 + \beta_{11} X_1^2 + \beta_{22} X_2^2 + \beta_{33} X_3^2 + \beta_{12} X_1 X_2 + \beta_{23} X_2 X_3 + \beta_{13} X_1 X_3 \quad (2)$$

Where Y is the percentage of EL yield, β_0 is the intercept/constant coefficient, β_1 , β_2 and β_3 are the linear coefficients, β_{11} , β_{22} and β_{33} are the quadratic coefficients, β_{12} , β_{13} and β_{23} are the interaction coefficient of each parameter and X_1 , X_2 and X_3 are the codes of independent input parameters.

2. Results and discussion

2.1. Physical and chemical properties of catalyst

N_2 sorption isotherms of pure carbon sphere, S-C and 10-40%Zn-S-C catalysts are shown in Fig. S2. One can see that all catalysts presented IUPAC type IV isotherms with a hysteresis loop of capillary condensation step at 0.4-0.8 P/P_0 , corresponding to the typical characteristics of mesoporous materials [2]. The isotherm of pure carbon sphere without subsistence of sulfonic group and zinc oxide showed a loop shape, which could be classified as the type H-3 hysteresis loop with slit-shaped pores. However, this obtained hysteresis loop style was changed into the type H-2 after carbon sphere was modified such as S-C and 10-40%Zn-S-C, suggesting the presence of ink-bottle porous structure [3]. The textural properties of prepared catalysts are summarized in Table S3. As expected, the BET surface area, pore volume and pore size of S-C was decreased to some extent with the increase in Zn loading amount from 10 to 40 wt.%, indicating that that surface and pore structures of S-C support were well covered by the dispersed Zn species.

The XRD pattern of prepared catalysts are shown in Fig. S3. The diffractogram of pure carbon sphere presented some broad crystalline peaks about 10–30° and 35-50°C, which was ascribed to the reflections on (002) and (101) planes of the amorphous carbon structure. After sulfonation process, the diffraction peak of S-C was shifted to higher 2-theta while intensity of peak was also clearly reduced, probably due to an enhanced disorder-graphitic carbon material [4,5]. In the cases of Zn loading (10-40 wt%), they presented main diffraction peaks of zinc oxide, which appeared at 31.8, 34.6, 36.3, 47.7, 56.7 and 62.9° [6].

The SEM-EDS mapping images of pure carbon sphere and S-C are shown in Fig. S4. Both samples had a spherical-like structure without any changing of morphology even though *in-situ* hydrothermal carbonization-sulfonation processes were applied. As shown in Fig. S5, after template-free solvothermal treatment process, zinc oxide nanorod was well deposited on the surface of S-C. Also, the increasing of Zn loading amount from 10 to 40 wt.% resulted in the growth of size of zinc oxide nanorod particle sizes. The reaction for the formation of ZnO nanorod on S-C catalyst (Zn-S-C) are shown as follows:



During solvothermal treatment, zinc oxide nanorod was gradually formed with the increase in pH value via decomposition of zinc acetate dihydrate into acetic acid and water at temperature of >120 °C. As such, –OH groups of zinc hydroxide crystals were further adsorbed on the S-C surface through hydrogen bonding. For EDS mapping images, as shown in Figures S2 and 4, S and Zn elements were well distributed on the surface of supports. This should be beneficial for catalytic conversion of sucrose into EL.

The NH₃-TPD profiles of prepared catalysts are shown in Fig. S6. Two NH₃ desorption peaks consisting of weak acid and strong acid sites in a temperature range of 125 to 450 °C were observed for S-C without Zn loading [7]. After Zn loading process, the NH₃ desorption peaks were shifted to higher temperature while the intensity peaks at low temperature were

also increased to some extent with the increase in Zn loading amount from 10 to 40 wt.%. This different distribution of acid sites resulted from interaction between zinc oxide with S-C via substitution process. Table S3 shows the catalyst acidity quantified from the peak area of NH₃-TPD. One can see that the acidity of Zn-S-C catalyst was consistently increased after increase in Zn loading amount. Here, the high acidity of catalyst should be beneficial for hydrolysis, isomerization, dehydration, and etherification reactions. The TG-DTG profiles of S-C and Zn-S-C are shown in Fig. S7. The different thermal decomposition behaviors were evidently appeared. For S-C catalyst without Zn loading, the temperature range around 250-450 °C was generally attributed to decomposition of sulfonic group from carbon support [8]. Interestingly, after Zn loading process, the thermal decomposition range was shifted into higher temperature, indicating that interaction between sulfonic and zinc group promoted the catalyst stability which was reasonable for reaction in this study.

3.2. Experimental analysis for conversion of sucrose into EL

The EL yield derived from 2⁴ factorial design with sixteen experiments is shown in Table S1. It is found that the range of EL yield about 11 to 67% was obtained from ultrasound-assisted one-pot conversion of sucrose over 30%Zn-S-C catalyst. To screen the significant factors, normal probability plots was primarily studied as shown in Fig. S8. One can see that three significant factors such as catalyst loading amount (wt.%), reaction time (min), reaction temperature (°C) including their interactions were found. The order of three factor for EL production was catalyst loading amount > reaction time > reaction temperature. It should be mentioned here that the range of THF adding amount (0.25 to 0.50 mol) had non-significant effect for enhancing the selective formation of EL. According to Le Chatelier's principle, to shift the equilibrium forward to wanted product, the excess amount of solvent was extremely desired. Here, the presence of THF solvent was very importance for acidic reaction conditions, especially for dehydration-etherification-ring opening through behavior in prompt region of H

atoms at the OH groups while the side-reactions could be well suppressed [9]. However, it should be considered the problem of phase separation when over amount of THF was used. Meanwhile, large amount of THF molecules could be covered on the surface of catalyst, leading to fast deactivation together with inactive. Therefore, lowest THF adding amount of 0.25 mol was certainly fixed for all experiment after this. Table S4 presents the analysis of variance (ANOVA) at confidence level of 95% with $F_{0.05}$. Here, the observed factors had significant effect when their F-values were more than 5.32 value. The maximum and minimum F-values derived from catalyst loading and reaction temperature were 785.39 and 234.22, respectively. The result of ANOVA was in well agreement with estimated effect of normal probability as shown in Fig. S8. Based on above results, the predicted EL yield was calculated via linear regression model consisting of low and high levels as follows in Equation (1):

$$Y = 37.29 + 11.456X_1 + 7.994X_2 + 6.256X_3 + 1.044X_1X_3 + 0.981X_2X_3 + 2.019X_1X_2X_3 \quad (1)$$

Where Y is the EL yield (%), X_1 is the catalyst loading amount (wt.%), X_2 is the reaction time (min) and X_3 is the reaction temperature ($^{\circ}\text{C}$).

The normal probability plot of residual value and distribution plot of residual are shown in Fig. S9. Here, the applied linear regression model had high dependability and precision based on a good linearity with $R^2 > 0.9$ while the distribution of residue value was in the range of $\pm 1.5\%$. From results of 2^4 factorial design, a lowest THF amount was selected for further study on optimization of EL production via Box-Behnken design. The EL yield derived from Box-Behnken design with fifteen experiments is shown in Table S2. The predicted EL yield was calculated via the quadratic regression model consisting of low, medium and high levels as follows in Equation (2):

$$Y = 69.800 + 12.013X_1 + 9.563X_2 + 7.725X_3 - 15.725X_1^2 - 14.325X_2^2 - 20.000X_3^2 + 6.500X_1X_2 + 4.375X_1X_3 + 3.225X_2X_3 \quad (2)$$

Where Y is the EL yield (%), X_1 is the catalyst loading amount (wt.%), X_2 is the reaction time (min) and X_3 is the reaction temperature ($^{\circ}\text{C}$).

The predicted yield of EL was calculated from Equation (2) and the result is shown in Table S2. As shown in Fig. S10, $R^2 > 0.95$ with variability of 98.61% for polynomial investigation was obtained from the plot of observed yield versus predicted yield of EL, suggesting that predicted yield of EL was well close to observed yield based on term of high accuracy. To know more details on the interaction of each independent input factor, the optimization using response surfaces is shown in Fig. S11. The interaction between catalyst loading amount with reaction time for ultrasound-assisted one-pot conversion of sucrose into EL over 30%Zn-S-C catalyst at a constant reaction temperature of $90\text{ }^{\circ}\text{C}$ (medium level) is shown in Fig S11A. The increasing of catalyst loading amount from 35 to 56 wt.% promoted the formation of EL whereat percent yield increased from 24.7 to 46.4%. This phenomenon should be ascribed in accreting of available active sites and collision rate between sucrose and catalyst, leading to facile reaction process. However, when catalyst loading amount of >53 wt.% was utilized, the formation rate based on EL yield was reduced to some extent, probably due to the resistance effect in mass transfer occurred from too high viscous slurries and poor mixing in mixture solution. Moreover, large catalyst dosages may be accelerated more side reactions such as polymerization reactions of EL and intermediates into humins [10].

The possible reaction pathway for formation of EL and other products from sucrose conversion are shown in Fig. S12. The first step was the hydrolysis process of sucrose molecule to glucose and fructose intermediates on the sulfonic groups-Brønsted acid sites. Here, glucose molecule could be further converted into fructose molecules via isomerization process on the zinc groups-Lewis acid sites. Then, 5-HMF was produced via hydrolysis of fructose [11]. Meanwhile, fructose molecules might be attacked by ethanol to form ethyl fructoside through ethanolysis and dehydration before further 5-EMF creation. Lastly, 5-HMF etherification and

5-EMF ring-opening reactions were occurred to produce EL product. For this novel Zn-S-C catalyst, the zinc element could act as the Lewis acid site for improving the glucose isomerization. On the other hand, the zinc atom in the Zn-S-C catalyst was enveloped by water complex ions, which could be further hydrolyzed to generate the protons (H^+), resulting in high ability to accept and release electrons, as well as high proton mobility. This generated H^+ was highly beneficial for EL via catalyzing the hydrolysis, dehydration, etherification and ring-opening. More interestingly, in this our process, ultrasonic application could well facilitate on interfacial area and mass transfer through cavitation bubble magnitudes and energy hotspots, leading to the sucrose towards a fast reaction rate [12]. As known that ultrasound can crack the O–H bond in water molecule to produce hydroxyl and hydrogen radicals ($H_2O/\bullet OH + \bullet H$), which can attack the chains in carbohydrate, resulting in more radicals and oxidizing species such as ozone and hydrogen peroxide which could effectively promote hydrolysis and dehydration [13]. These oxidizing species could effectively promote hydrolysis and dehydration of sucrose into specific intermediates. It should be noted that unwanted products such as humins could be easily formed via polymerization reactions when inappropriate conditions were applied. For possible recycling in practical large-scale process, biphasic reaction system and *in-situ* extraction technology were applied in this study. Here, sodium chloride was mixed to escalate the immiscibility between THF and ethanol/water phases, leading to *in-situ* extraction of two layer finally [14].

As shown in Fig. S11B, the highest EL yield about ~73% was derived from interaction between a catalyst loading amount of 56 wt.% with a reaction temperature of 96 °C at a constant reaction time of 55 min (medium level). For Figure 8C, considering at the effects of reaction time and temperature, the highest EL yield was found at 96°C for 65 min at constant catalyst loading amount of 50 wt.%. The EL yield was evidently reduced after approximately reaction time of >65min and reaction temperature of >100 °C were applied, suggesting that that EL

molecules were further converted into unwanted products such as humins via side-reactions [15]. This phenomenon could be distinguished in product color by changing from brown to black color. As observed in Figs. S11B and S11C, reaction temperature used in this study must not exceed 100 °C even through high reaction temperature was usually required as a positive effect since reaction used for EL formation was endothermic nature, resulting from contribution of ultrasonic energy. It is also probable that at too high reaction temperature, THF and ethanol solvents might be converted from liquid into vapor phases, leading to less solvent available in the reaction environment.

Based on response surface analysis, the optimization at equilibrium conditions could be systematically predicted through Box-Behnken design with quadratic regression model. Here, the optimum conditions such as catalyst loading amount of 57.8 wt.%, THF amount of 0.25 mol, reaction time of 67 min and reaction temperature of 98.7 °C, obtaining a highest predicted EL yield of 76.4%. To identify the exactitude for this design, veritable experimental was investigated through obtained optimum conditions for three duplicates. It is found that an average yield of EL (78.3%) was practically achieved.

REFERENCE

- (1) Karnjanakom, S.; Kongparakul, S.; Chaiya, C.; Reubroycharoen, P.; Guan, G.; Samart, C. Biodiesel production from *Hevea brasiliensis* oil using SO₃H-MCM-41 catalyst. *J. Environ. Chem. Eng.* 2016, 4, 47–55.
- (2) Zhong, R.; Yu, F.; Schutyser, W.; Liao, Y. Clippel, F. D. Peng, L.; Sels, B. F. Acidic mesostructured silica-carbon nanocomposite catalysts for biofuels and chemicals synthesis from sugars in alcoholic solutions. *Appl. Catal., B* 2017, 206, 74–88.
- (3) Karnjanakom, S.; Bayu, A.; Hao, X.; Kongparakul, S.; Samart, C.; Abudula, A.; Guan, G. Selectively catalytic upgrading of bio-oil to aromatic hydrocarbons over Zn, Ce or

- Ni-doped mesoporous rod-like alumina catalysts. *J. Mol. Catal. A Chem.* 2016, 421, 235–244.
- (4) Malins, K.; Kampars, V.; Brinks, J.; Neibolte, I.; Murnieks, R. Synthesis of activated carbon based heterogenous acid catalyst for biodiesel preparation. *Appl. Catal., B* 2015, 176, 553–558.
- (5) Mun, D.; Vo, A. T. H.; Kim, B.; Shul, Y. G.; Cho, J. K. Solventless esterification of fatty acids with trimethylolpropane using sulfonated amorphous carbons derived from wood powder. *Catal. Commun.* 2017, 96, 32–36.
- (6) Ray, P. G.; Das, M.; Wan, M.; Jacob, C.; Roy, S.; Basak, P.; Dhara, S. Surfactant and catalyst free facile synthesis of Al-doped ZnO nanorods – An approach towards fabrication of single nanorod electrical devices. *Appl. Surf. Sci.* 2020, 512, 145732.
- (7) Goncalves, M.; Castro, C. S.; Oliveira, L. C. A.; Carvalho, W. A. Green acid catalyst obtained from industrial wastes for glycerol etherification. *Fuel Process. Technol.* 2015, 138, 695-703.
- (8) Zhao, Y.; Chen, H.; Huang, Y.; Zhao, Y.; Fu, Y.; Shen, J. Sulfonated carbon materials with hydrophilic and lipophilic properties. *J. Energy Chem.* 2014, 23, 156-163.
- (9) Yang, Y.; Abu-Omar, M. M.; Hu, C. Heteropolyacid catalyzed conversion of fructose, sucrose, and inulin to 5-ethoxymethylfurfural, a liquid biofuel candidate. *Appl. Energy* 2012, 99, 80-48.
- (10) Song, D.; Sun, Y.; Zhang, Q.; Zhang, P.; Guo, Y.; Leng, J. Fabrication of propylsulfonic acid functionalized SiO₂ core/PMO shell structured PrSO₃H-SiO₂@Si(R)Si nanospheres for the effective conversion of D-fructose into ethyl levulinate. *Appl. Catal., A* 2017, 546, 36–46.
- (11) Zhou, P.; Zhang, Z. One-pot catalytic conversion of carbohydrates into furfural and 5-hydroxymethylfurfural. *Catal. Sci. Technol.* 2016, 6, 3694-3712.

- (12) Zou, J.; Nguyen, N.; Biers, M.; Sun, G. Conformational Changes of Soy Proteins under High-Intensity Ultrasound and High-Speed Shearing Treatments. *ACS Sustainable Chem. Eng.* 2019, 7, 8117-8125.
- (13) Shi, W.; Jia, J.; Gao, Y.; Zhao, Y. Influence of ultrasonic pretreatment on the yield of bio-oil prepared by thermo-chemical conversion of rice husk in hot-compressed water. *Bioresour. Technol.* 2013, 146, 355–362.
- (14) Chen, D.; Liang, F.; Feng, D.; Xian, M.; Zhang, H.; Liu, H.; Du, F. An efficient route from reproducible glucose to 5-hydroxymethylfurfural catalyzed by porous coordination polymer heterogeneous catalysts. *Chem. Eng. J.* 2016, 300, 177–184.
- (15) Dee, S. J.; Bell, A. T. A Study of the Acid-Catalyzed Hydrolysis of Cellulose Dissolved in Ionic Liquids and the Factors Influencing the Dehydration of Glucose and the Formation of Humins. *ChemSusChem* 2011, 4, 1166-1173.

Table S1 Experimental conditions and EL yield derived from 2⁴ factorial design.^a

Run	X ₁ (wt.%)	X ₂ (min)	X ₃ (°C)	X ₄ (mol)	EL yield (%)
1	35 (-1)	30 (-1)	60 (-1)	0.25 (-1)	11.5
2	65 (1)	30 (-1)	60 (-1)	0.25 (-1)	36.3
3	35 (-1)	80 (1)	60 (-1)	0.25 (-1)	32.8
4	65 (1)	80 (1)	60 (-1)	0.25 (-1)	47.3
5	35 (-1)	30 (-1)	120 (1)	0.25 (-1)	23.4
6	65 (1)	30 (-1)	120 (1)	0.25 (-1)	45.4
7	35 (-1)	80 (1)	120 (1)	0.25 (-1)	37.6
8	65 (1)	80 (1)	120 (1)	0.25 (-1)	66.7
9	35 (-1)	30 (-1)	60 (-1)	0.50 (1)	11.7
10	65 (1)	30 (-1)	60 (-1)	0.50 (1)	36.6
11	35 (-1)	80 (1)	60 (-1)	0.50 (1)	26.5
12	65 (1)	80 (1)	60 (-1)	0.50 (1)	45.6
13	35 (-1)	30 (-1)	120 (1)	0.50 (1)	24.8
14	65 (1)	30 (-1)	120 (1)	0.50 (1)	44.7
15	35 (-1)	80 (1)	120 (1)	0.50 (1)	38.4
16	65 (1)	80 (1)	120 (1)	0.50 (1)	67.4

^a The parameters are coded as follows: X₁ = catalyst loading amount (wt.%), X₂ = reaction time (min), X₃ = reaction temperature (°C) and X₄ = THF amount (mol).

Table S2 Experimental conditions and EL yields derived from Box-Behnken design.^a

Run	X ₁ (wt.%)	X ₂ (min)	X ₃ (°C)	EL yield (%)	
				Observed	Predicted
1	35 (-1)	30 (-1)	90 (0)	23.1	24.7
2	65 (1)	30 (-1)	90 (0)	35.2	35.7
3	35 (-1)	80 (1)	90 (0)	31.3	30.8
4	65 (1)	80 (1)	90 (0)	69.4	67.8
5	35 (-1)	55 (0)	60 (-1)	22.1	18.7
6	65 (1)	55 (0)	60 (-1)	36.3	34.0
7	35 (-1)	55 (0)	120 (1)	23.1	25.4
8	65 (1)	55 (0)	120 (1)	54.8	58.2
9	50 (0)	30 (-1)	60 (-1)	19.6	21.4
10	50 (0)	30 (-1)	60 (-1)	30.2	34.1
11	50 (0)	80 (1)	120 (1)	34.3	30.4
12	50 (0)	80 (1)	120 (1)	57.8	56.0
13	50 (0)	55 (0)	90 (0)	69.9	69.8
14	50 (0)	55 (0)	90 (0)	69.4	69.8
15	50 (0)	55 (0)	90 (0)	70.1	69.8

^a The parameters are coded as follows: X₁ = catalyst loading amount (wt.%), X₂ = reaction time (min) and X₃ = reaction temperature (°C).

Table S3 Physicochemical properties of various catalysts.

Catalyst	Surface area ^a (m ² /g)	Pore volume ^b (cm ³ /g)	Pore size ^b (nm)	Acid amount ^c (mmol/g)	Zn content ^d (wt.%)	S/Zn ratio ^e
C	135	0.84	10.5	0.34	-	-
S-C	121	0.69	9.7	3.14	-	-
10%Zn-S-C	108	0.55	8.4	3.35	10.2	0.0328
20%Zn-S-C	97	0.42	7.2	3.94	19.7	0.0200
30%Zn-S-C	84	0.35	5.8	4.22	29.4	0.0144
40%Zn-S-C	66	0.23	3.1	4.59	38.7	0.0119
Spent	86	0.38	5.9	3.87	27.9	0.0132
30%Zn-S-C ^e						
30%Zn-Amberlyst-35	26	0.19	24.1	4.78	29.7	-

^a BET method.

^b BJH method.

^c Back titration method.

^d ICP method.

^e Spent catalyst (After recycling test for 10 cycles).

Table S4 Analysis of variance (ANOVA) determined from 2⁴ factorial design for ultrasonic-assisted conversion of sucrose into EL over 30%Zn-S-C catalyst.^a

Source of variation	Sum of square	Degree of freedom	Mean square	F _{value}	F _{critical}
X ₁	2099.93	1	2099.93	785.39	
X ₂	1022.40	1	1022.40	382.38	
X ₃	626.25	1	626.25	234.22	
X ₄	1.76	1	1.76	0.66	5.32
X ₁ X ₃	17.43	1	17.43	6.52	
X ₂ X ₃	15.41	1	15.41	5.76	
X ₁ X ₂ X ₃	65.21	1	65.21	24.39	
Error	21.39	8	2.67		
Total	3869.77	15			

^a The parameters are coded as follows: X₁ = catalyst loading amount (wt.%), X₂ = reaction time (min) and X₃ = reaction temperature (°C).

Table S5 Catalytic comparison of Zn-C-S and representative catalysts for EL production.

Entry	Catalyst	Substrate/Solvent	Reaction conditions	EL yield (%)	Ref.
1	SO ₃ H-SBA-15	Sucrose/Ethanol	Ace pressure system: 140 °C for 24 h	27.0	[12]
2	AC-Fe-SO ₃ H	Sucrose/Ethanol	Solvothermal system: 200 °C for 3 h	29.0	[13]
3	WS ₂	Fructose/Ethanol	Microwave system: 160 °C for 30 min	23.0	[14]
4	Zn-S-C	Sucrose/ Ethanol+THF	Ultrasonic system at 220 W for 60% cycle: 98.7 °C for 67 min	78.3	This work
5	Zn-S-C	Cellobiose/ Ethanol+THF	Ultrasonic system at 220 W for 60% cycle: 98.7 °C for 67 min	54.1	This work
6	Zn-S-C	Glucose/ Ethanol+THF	Ultrasonic system at 220 W for 60% cycle: 98.7 °C for 67 min	66.2	This work
7	Zn-S-C	Fructose/ Ethanol+THF	Ultrasonic system at 220 W for 60% cycle: 98.7 °C for 67 min	80.2	This work
8	Zn-S-C	Sorbose/ Ethanol+THF	Ultrasonic system at 220 W for 60% cycle: 98.7 °C for 67 min	70.5	This work
9	Zn-S-C	Inulin/ Ethanol+THF	Ultrasonic system at 220 W for 60% cycle: 98.7 °C for 67 min	24.1	This work
10	Zn-S-C	Sucrose/ Ethanol+THF	Reflux system: 98.7 °C for 12 h	75.9	This work

Ref. from main paper

[12] S. Saravanamurugan, A. Riisager, *Catal Commun.* 2012, 17, 71-75.

[13] J. Zhang, J. Chen, *J. Energy Chem.* 2016, 25, 747-753.

[14] S. Quereshi, E. Ahmad, K. K. Pant, S. Dutta, *ACS Sustainable Chem. Eng.* 2020, 8, 1721-1729.

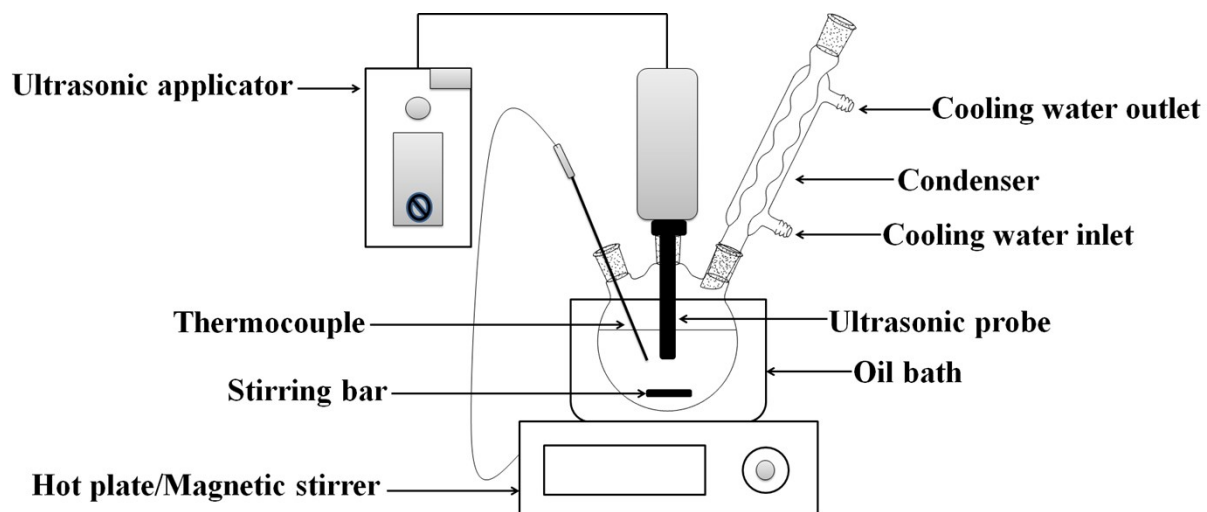


Fig. S1. Schematic diagram of the experimental set up for ultrasonic-assisted conversion of sucrose into EL.

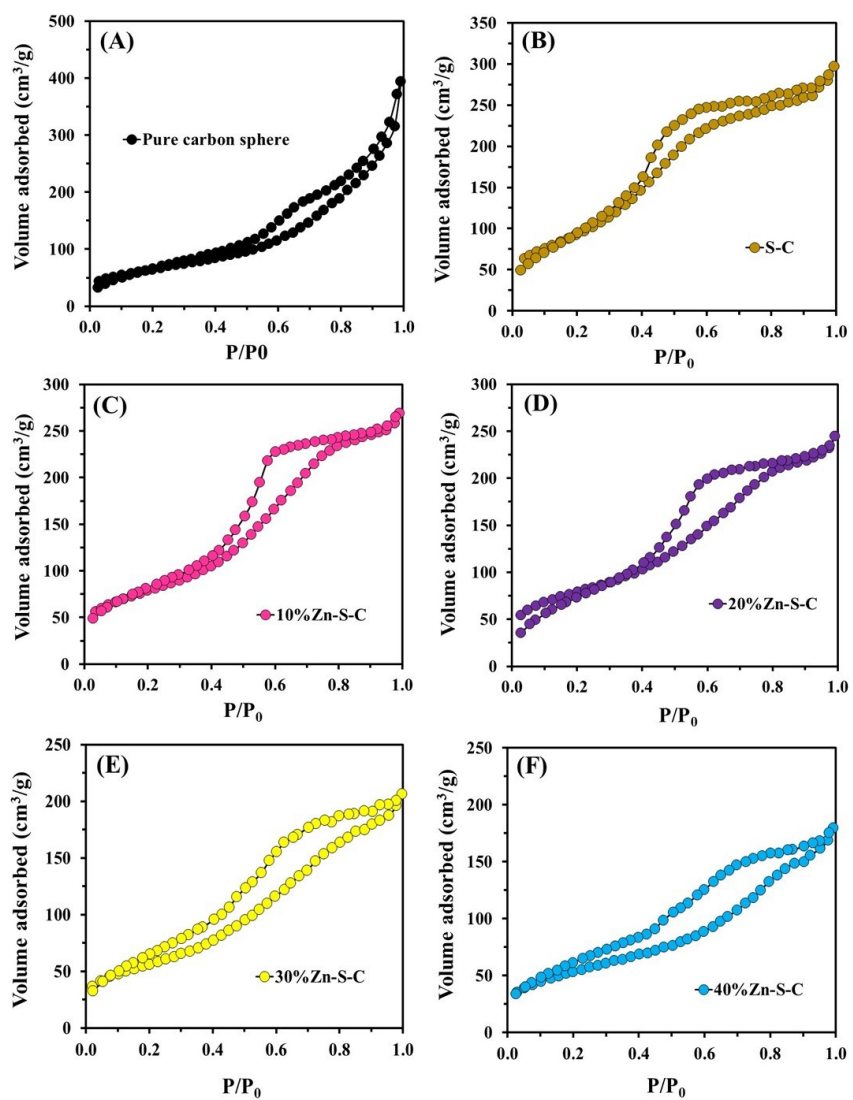


Fig. S2. N_2 sorption isotherms of (A) pure carbon sphere, (B) S-C, (C) 10%Zn-S-C, (D) 20%Zn-S-C, (E) 30%Zn-S-C and (F) 40%Zn-S-C.

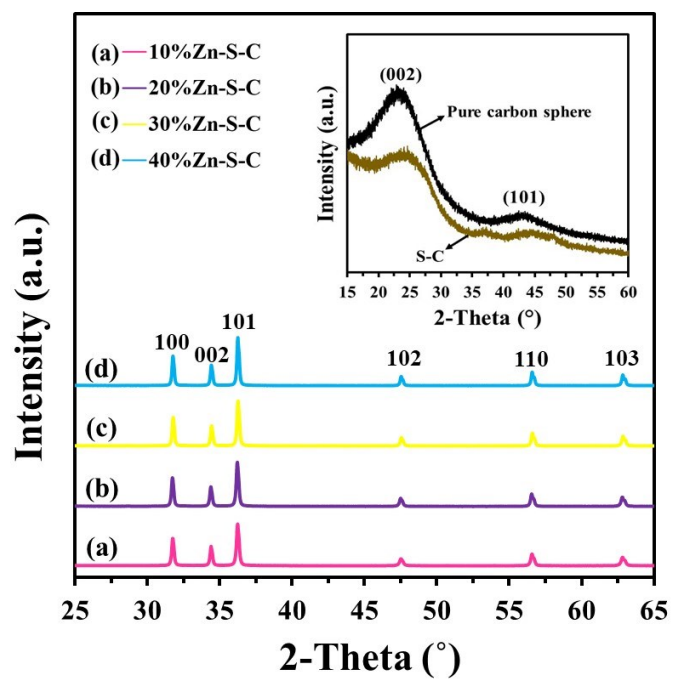


Fig. S3. XRD patterns of 10-40%Zn-S-C catalysts. Inset: XRD pattern of pure carbon sphere and S-C.

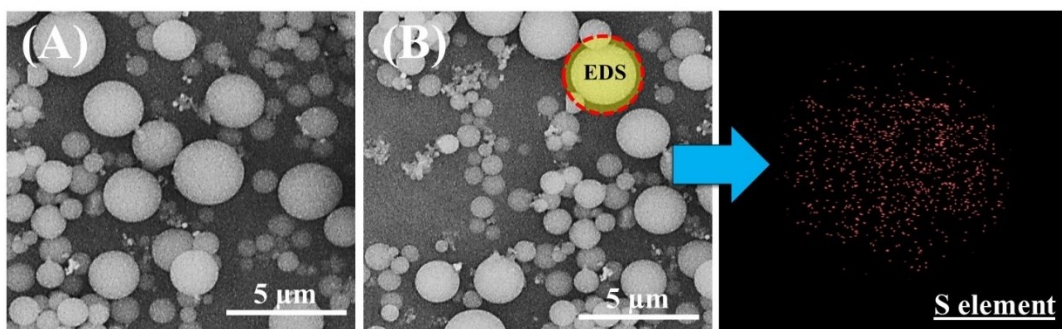


Figure S4. SEM-EDS mapping images of (A) pure carbon sphere and (B) S-C.

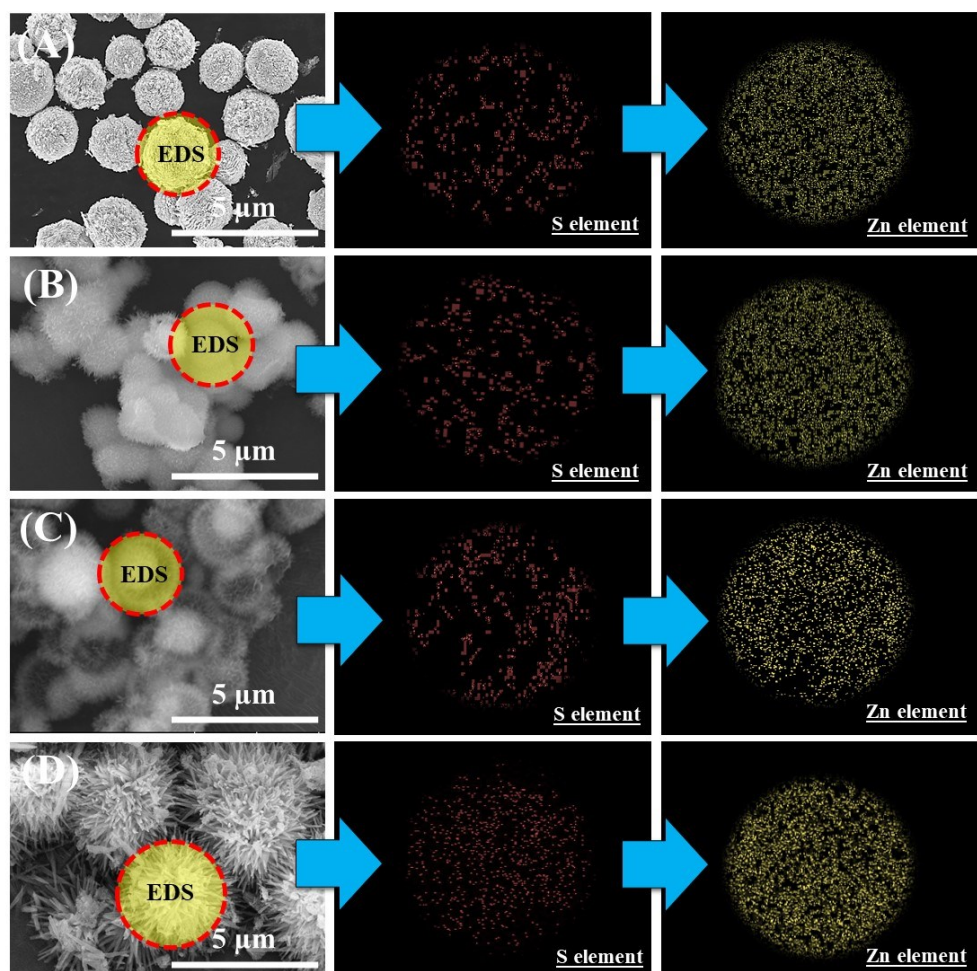


Fig. S5. SEM-EDS mapping images of (A) 10%Zn-S-C, (B) 20%Zn-S-C, (C) 30%Zn-S-C and (D) 40%Zn-S-C.

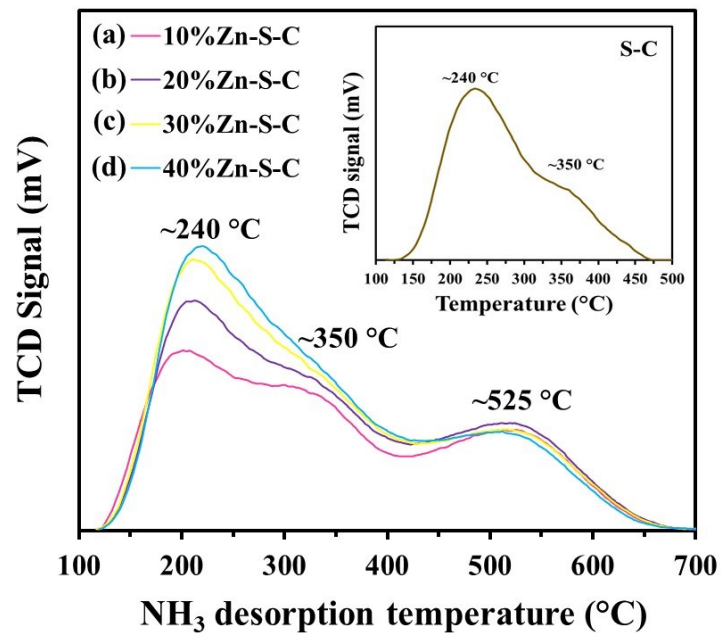


Fig. S6. NH₃-TPD profiles of 10-40%Zn-S-C catalysts. Inset: NH₃-TPD profile of S-C.

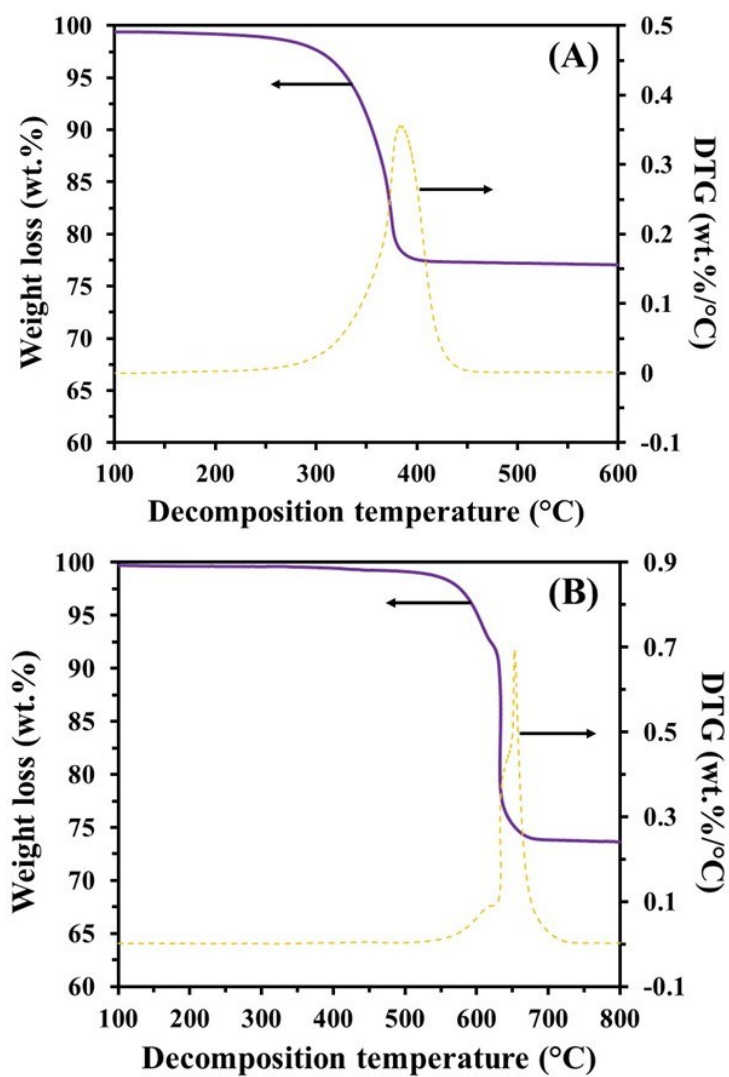


Fig. S7. TG-DTG profiles of (A) S-C and (B) 30%Zn-S-C.

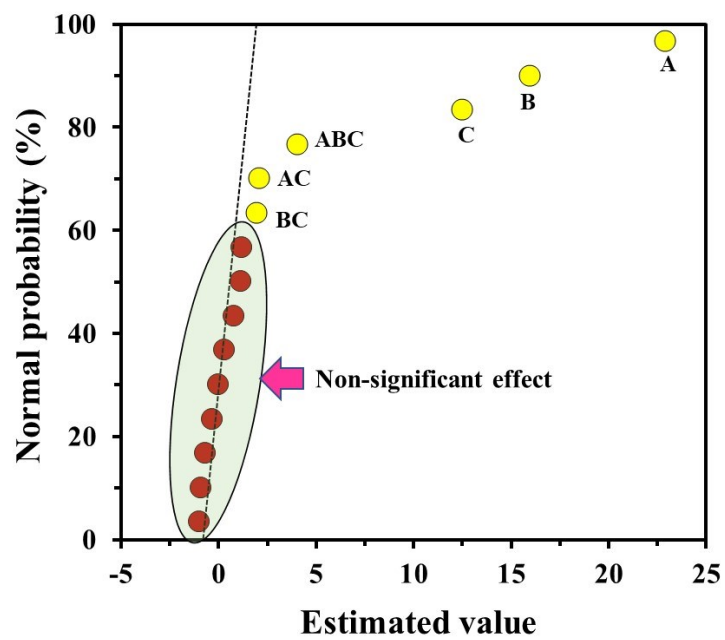


Fig. S8. Normal probability plot design for ultrasound-assisted one-pot conversion of sucrose into EL over 30%Zn-S-C catalyst.

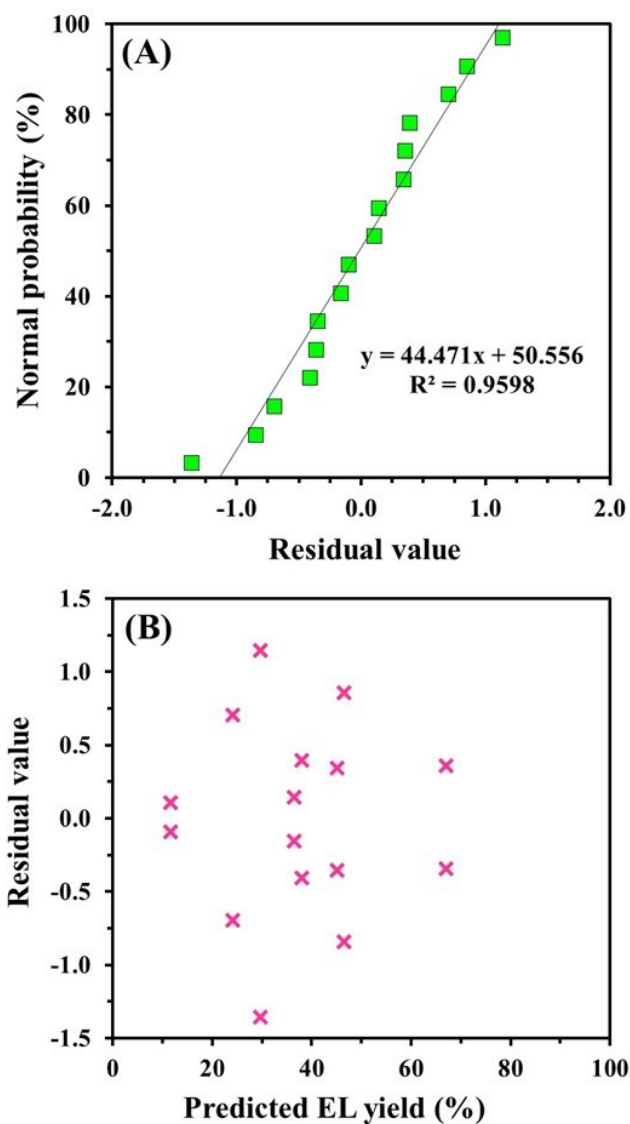


Fig. S9. (A) Normal probability plot of residual and (B) distribution plot of residual versus predicted EL yield determined from 2^4 factorial design for ultrasound-assisted one-pot conversion of sucrose into EL over 30%Zn-S-C catalyst.

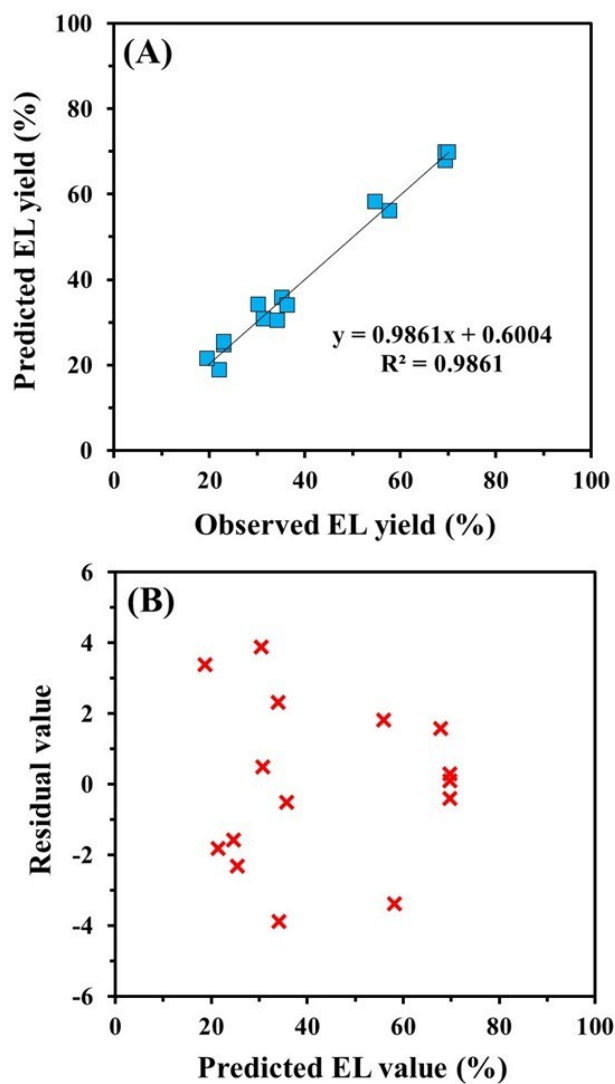


Fig. S10. (A) Plot of observed versus predicted values of EL yield and (B) distribution plot of residual value versus predicted EL yield determined from Box-Behnken design for ultrasound-assisted one-pot conversion of sucrose into EL over 30%Zn-S-C catalyst.

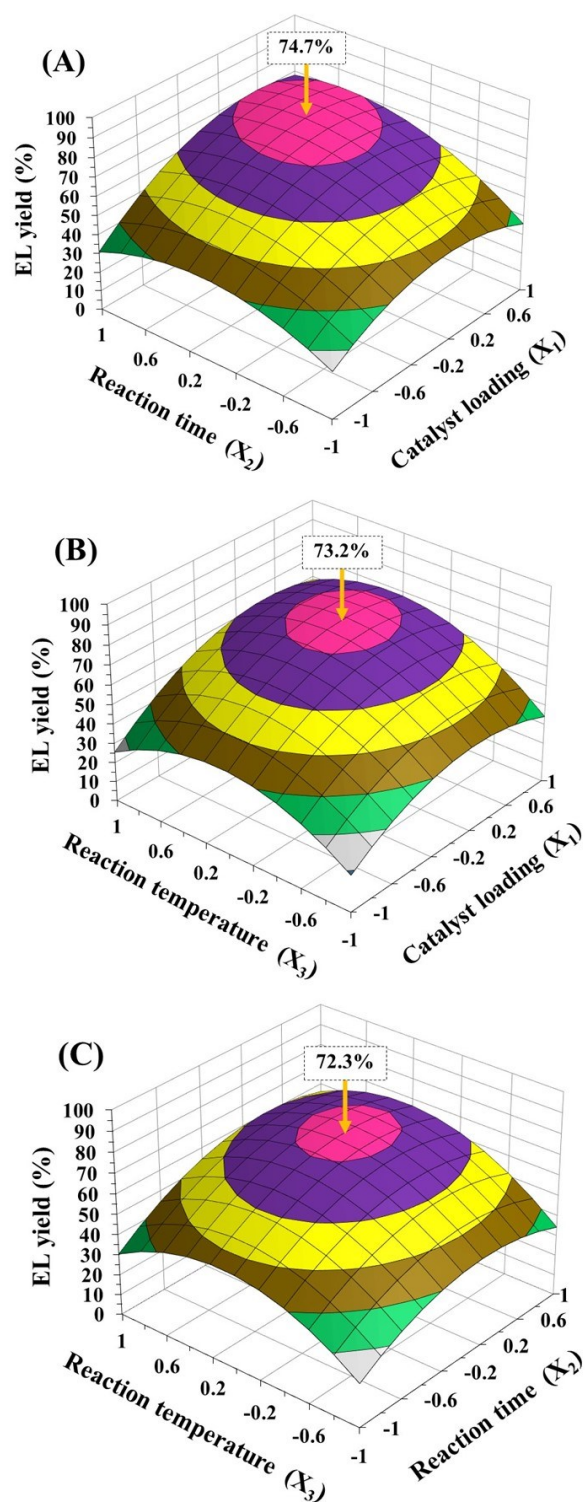


Fig. S11. Response surfaces determined from EL yield: (A) interaction effect of catalyst loading and reaction time, (B) interaction effect of catalyst loading and reaction temperature, and (C) interaction effect of reaction time and reaction temperature.

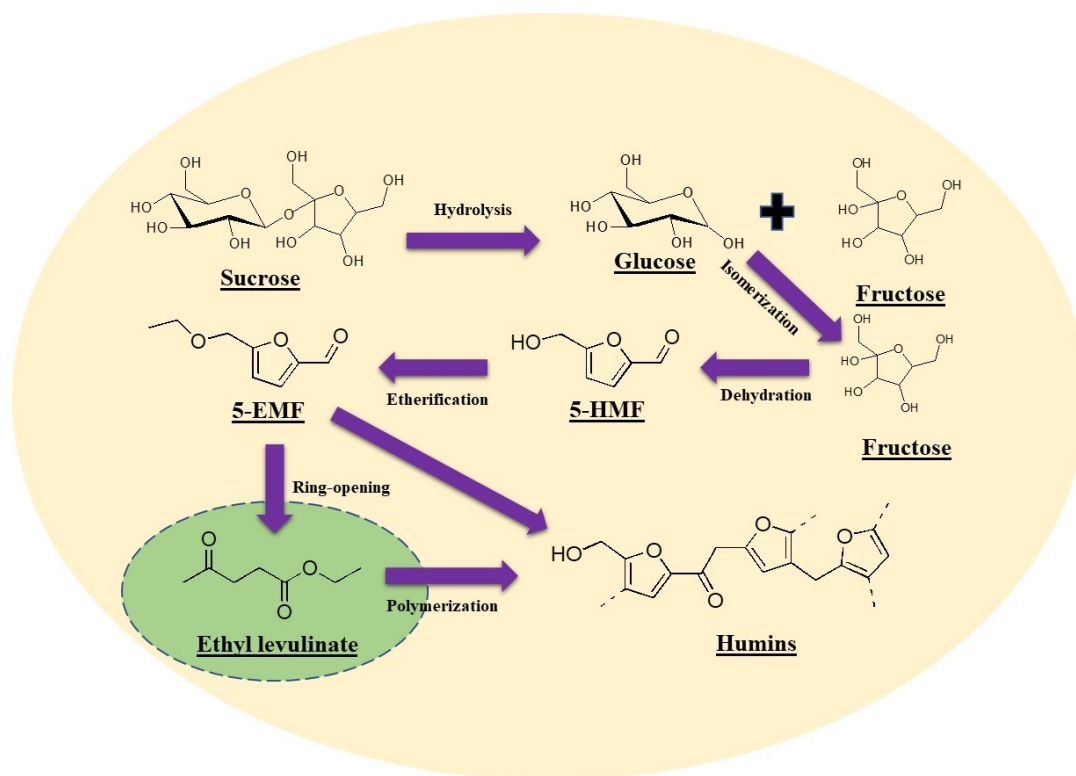


Fig. S12. Reaction pathway for ultrasound-assisted one-pot conversion of sucrose into EL and other products over Zn-S-C catalyst.

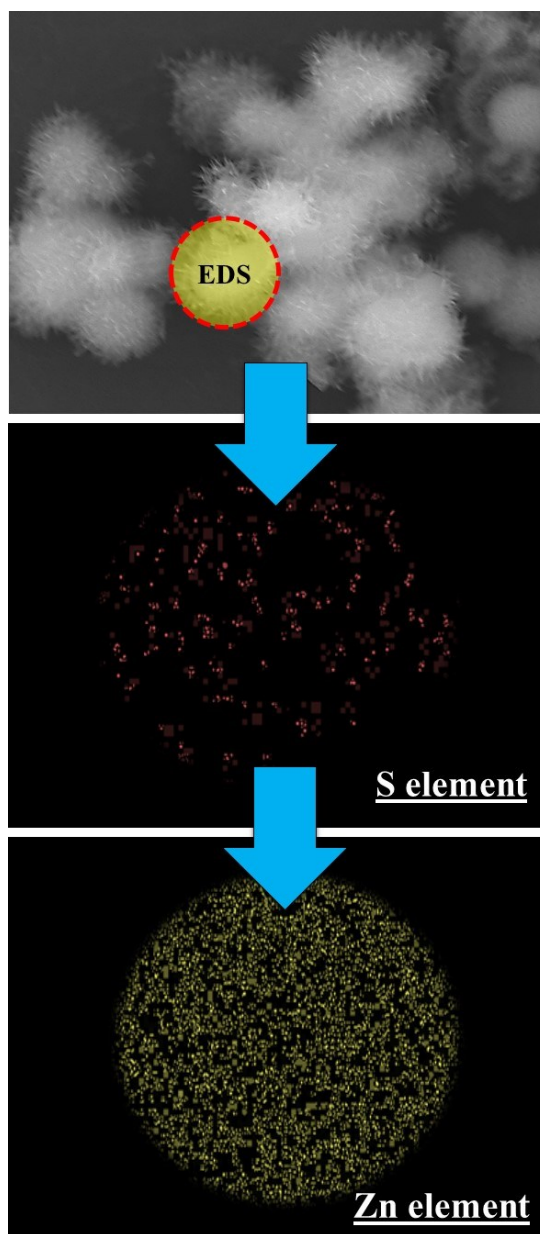


Fig. S13. SEM-EDS mapping images of spent 30%Zn-S-C catalyst after recycling test for 10 cycles.

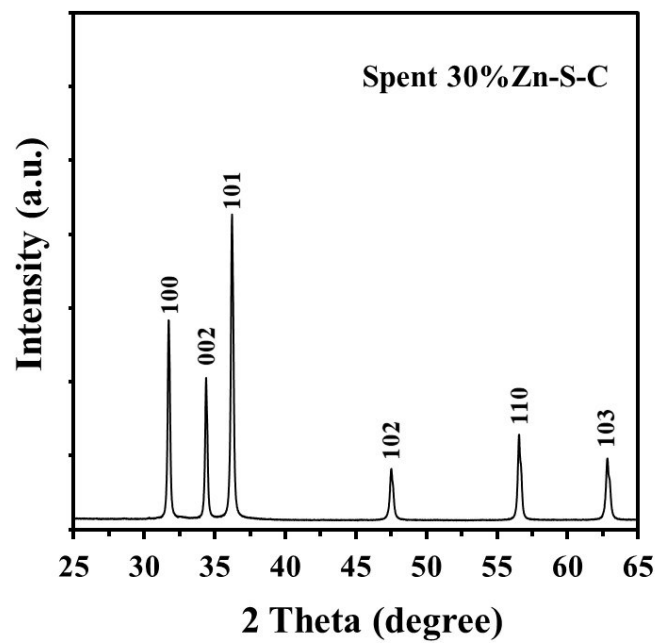


Fig. S14. XRD patterns of spent 30%Zn-S-C catalyst after recycling test for 10 cycles.

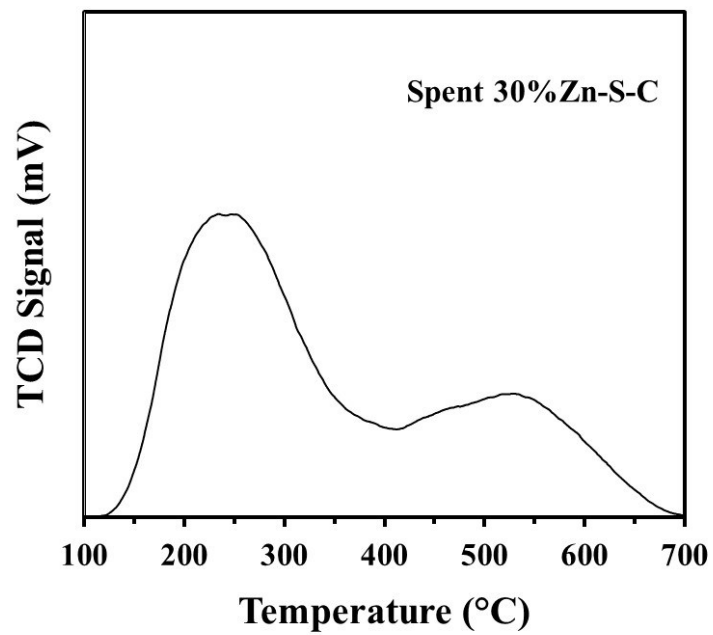


Fig. S15. NH₃-TPD profile of spent 30%Zn-S-C catalyst after recycling test for 10 cycles.

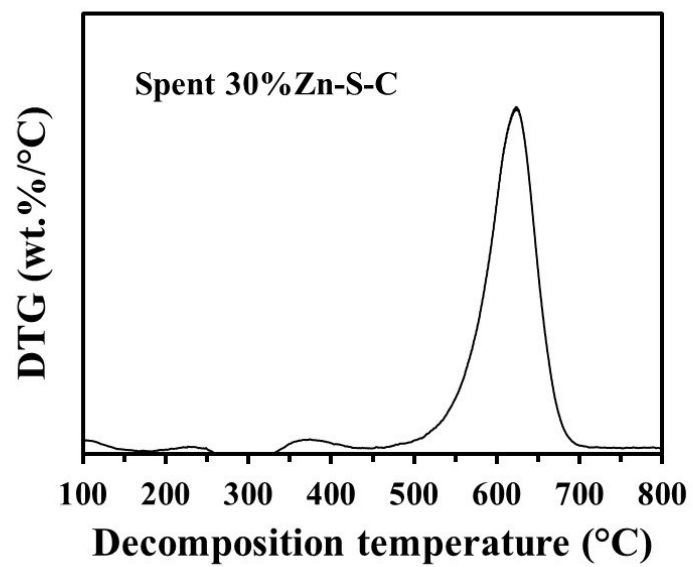


Fig. S16. DTG profile of spent 30%Zn-S-C catalyst after recycling test for 10 cycles.